Integrated geological, geophysical, and hydrological study of field-scale fault-zone cementation and permeability, Loma Blanca Fault Central New Mexico

By

Johnny Ray Hinojosa, Geology MSC Candidate

Peter Mozley, Professor of Sedimentology

TECHNICAL PROGRESS REPORT

Sub Award Q01864

June 2017

Funded by:

New Mexico Water Resources Research Institute

National Science Foundation

DISCLAIMER

The New Mexico Water Resource Research Institute and affiliated institutions make no warranties, express or implied, as to the use of the information obtained from this data product. All information included with this product is provided without warranty or any representation of accuracy and timeliness of completeness. Users should be aware that changes may have occurred since this data set was collected and that some parts of these data may no longer represent actual conditions. This information may be updated without notification. Users should not use these data for critical applications without a full awareness of its limitations. This product is for informational purposes only and may not be suitable for legal, engineering, or surveying purposes. The New Mexico Water Resource Research Institute and affiliated institutions shall not be liable for any activity involving these data, installation, fitness of the data for a particular purpose, its use, or analyses results.

ABSTRACT

The Loma Blanca fault is a Pliestocene age normal fault located within the Sevilleta National Wildlife Refuge in central New Mexico. The normal fault is an extensional feature of the Rio Grande Rift. It is believed that the fault is a barrier to subsurface fluid flow moving down-gradient towards the Rio Grande River. Previous work under a National Science Foundation grant conducted geophysical measurements in an attempt to visualize groundwater impoundment on the footwall (up-gradient) side of the fault. This study will build on the data collected and characterize the geology that influences fault-sealing characteristics. Thin sections have been made from outcrops on either side of the fault that include unconsolidated fluvial sediment as well as fully cemented sand near the fault deformation zone. Mercury intrusion porosimetry analyses were conducted on hanging wall and footwall samples from fully cemented and partially cemented section of the fault. Data indicate discernable differences in calculated porosity and permeability from two distinct styles of cementation. Core samples were recovered from seven boreholes and are will provide subsurface data to inform a 3-dimensional geologic model. Current work includes constructing a stratigraphic framework, core analysis, and creating a model that captures horizontal and lateral heterogeneity affecting subsurface cross-fault fluid flow.

Keywords: Fault, cementation, groundwater, fault-sealing, porosity, permeability, cross-fault fluid flow, mercury intrusion porosimetry

Contents

LIST OF FIGURES

JUSTIFICATION OF WORK

Two of the greatest impediments to predicting the impact of faults on fluid flow in the subsurface are: 1) fault seal models inadequately accounting for fault-zone cementation, and 2) a paucity of field-scale hydrologic data directly testing conceptual models of fault seal. Current approaches to predicting fault seal in the subsurface are mainly based upon variations in host rock lithology and throw (e.g., juxtaposition and entrainment effects). They do not account for fault-zone cementation, despite the widespread recognition that it is common and can dramatically decrease fault permeability [*Lindsay et al*., 1993; *Fristad et al*., 1997; *Fulljames et al*., 1997; *Welbon et al*., 1997; *Childs et al.*, 2002; *Yielding*, 2002; *Bretan et al*., 2003; *Manzocchi et al.,* 2010]. Although outcrop-scale conceptual models of fault-zone hydrogeology have advanced our understanding of fluid flow in complex systems, most numerical models of hydrogeologic systems require field- to regional-scale estimates for fault-zone permeability.

The goal of this study is a multi-year research endeavor that will incorporate elements of geology, geophysics and hydrology. The geology portion of the research will include thin section petrography, grain size analysis from outcrop samples, wellbore core and cutting analyses, and measured sections. Additionally, cross sections will be constructed to accurately represent distinct hydogeologic facies adjacent to the fault. Cross sections, measured sections, and lithology data from core and cuttings will ultimately contribute to a local 3-dimensional geologic model

hydrologists will use for flow simulations using numerical analysis. Current research has examined petrographic samples and evaluated mercury intrusion porosimetry data during the WRRI timeframe.

Preliminary reconnaissance of the field site located within the Sevilleta Wildlife Refuge identified locations for thin section sample collection and areas along the cemented portion of the Loma Blanca fault that were ideal candidates for mercury intrusion porosimetry analysis. Conclusions from these initial observations have shaped the understanding of the subsurface with relation to lithology and permeability characteristics.

METHODS

Petrography

Petrographic analyses were conducted using an Olympus CX31 polarized light microscope. Photomicrographs of thin sections taken with a Diagnostic Instruments 2x adapter and Canon EOS Rebel T2i camera mounted to the microscope**.** All thin sections were mounted on a glass slide, cut to a standard thickness of 30 microns, and treated with blue epoxy to highlight primary and secondary porosity. Coverslips were not prepared for the thin sections, as they will be processed using an electron microprobe for future elemental analyses. Polarized and cross-polarized light were used to identify minerals and cements within the thin section.

Framework grains such as monocrystalline quartz, polycrystalline quartz, feldspars, volcanic lithic grains, heavy minerals, phyllosillicates, and siliciclastic sedimentary grains were identified in samples taken adjacent to the fault damage zone and in unconsolidated sediment on the footwall side of the fault. Classification of framework grains followed criteria set forth by Dickenson (1970), Ingersoll and Suzek (1979) and Folk (1980). Future work will contribute point counts and ternary diagrams to add quantitative data to the initial qualitative analyses. While the framework grains were genetically similar among the sedimentary samples, they varied morphologically. Grain size, sorting distribution, and composition were used to determine porosity and permeability relationships.

Mercury Intrusion Porosimetry

Mercury intrusion porosimetry (MIP) was performed on a Micromeritics AutoPore IV 9500 Series porosimeter. Raw samples from outcrop were cut down and fashioned into 2.54 cm (1.0 in) plugs in order to fit the inner diameter of the porosimeters penetrometer bulb. Prior to analysis, samples were dried at 100˚C in order to remove residual moisture in pore space. Samples were taken within the deformation zone of the fault, so bedding was not discernable. Thus jacketing the plugs with epoxy for capillary and transport properties in the direction of bedding was not performed. Breakthrough capillary pressure (also called bubbling pressure or sealing pressure) is the pressure at which a continuous filament of mercury extends across a MIP sample, or equivalently, the pressure when the non-wetting phase first appears on the outlet side of a sample plug (Katz and Thompson, 1987;

Catalan et. al, 1992; Dewhurst et al., 2002). For these analyses, it was estimated by identifying the point on the cumulative mercury saturation versus pressure curve with maximum inflection upwards.

Four outcrop samples were selected for this procedure, two from the hanging wall, and two from the footwall. The samples were also oriented spatially so that they represent different styles of fault cementation. Hanging wall and footwall samples were taken from a section of the fault that exhibits high amounts of continuous cementation, and two other hanging wall and footwall samples were taken from an area where cementation becomes more sporadic. The importance of capturing different levels of cementation, from continuous cement to blocky concretionary cement, rests in the discrete relationships between porosity, permeability, and lithology.

PRINCIPLE FINDINGS

Petrography of samples LBF_0212_1A and LBF_0212_1B identified botryoidal opal (Fig. 1 & 2) as the primary intergranular cement. The cement exhibits a rounded, concentric growth morphology emanating from host grains as authigenic overgrowths. Opal appears as off-white translucent in polarized light and opaque in cross-polarized light with no observed birefringence due to the minerals isotropic nature. This finding was unexpected, as the original hypothesis identified calcium carbonate as the primary cement influencing sediment induration and fault relief.

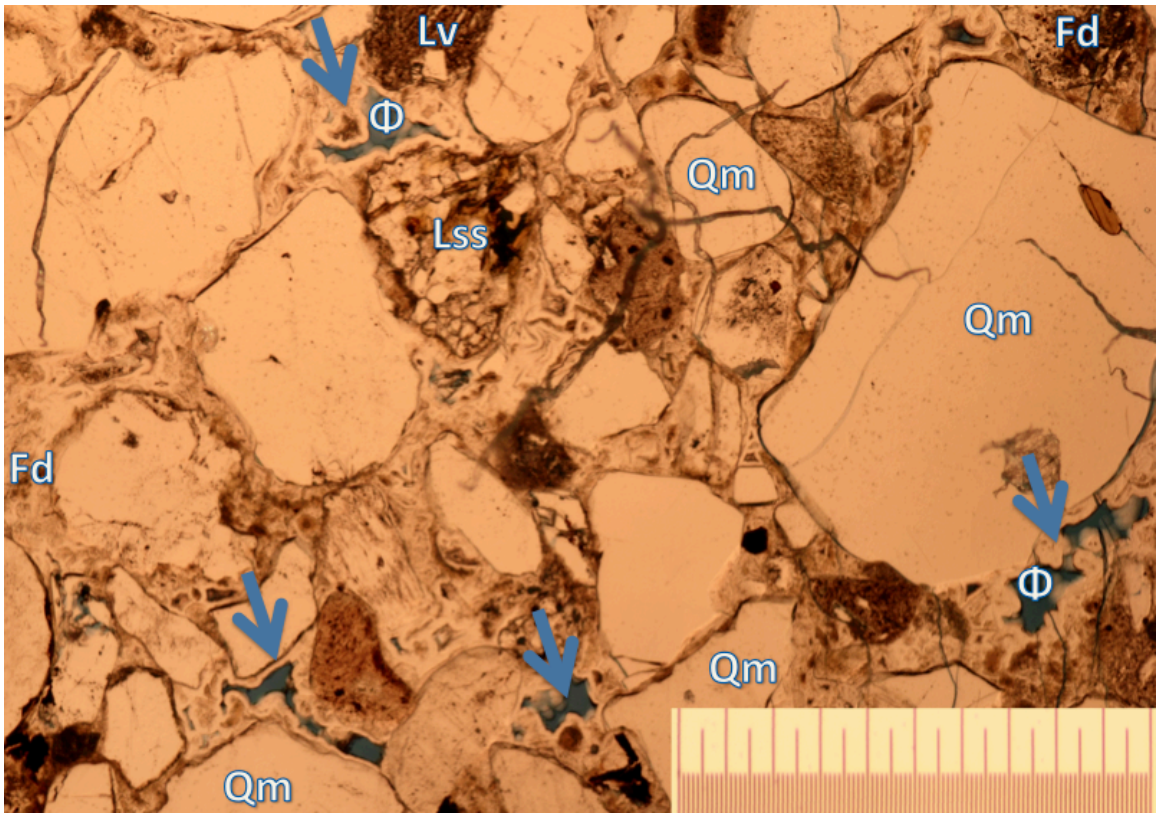

Figure 1 – Polarized photomicrograph of sample LBF_0212_1A with 8x magnification. The sample is composed of monocrystalline quartz (QM), feldspars that show levels of sericsite alteration (Fd), lithic volcanic fragments (Lv), and lithic sedimentary fragments (Lss). The ϕ symbol over blue epoxy indicates areas of intergranular porosity. Blue arrows highlight botryoidal opal cementation. Scale bar is 1mm.

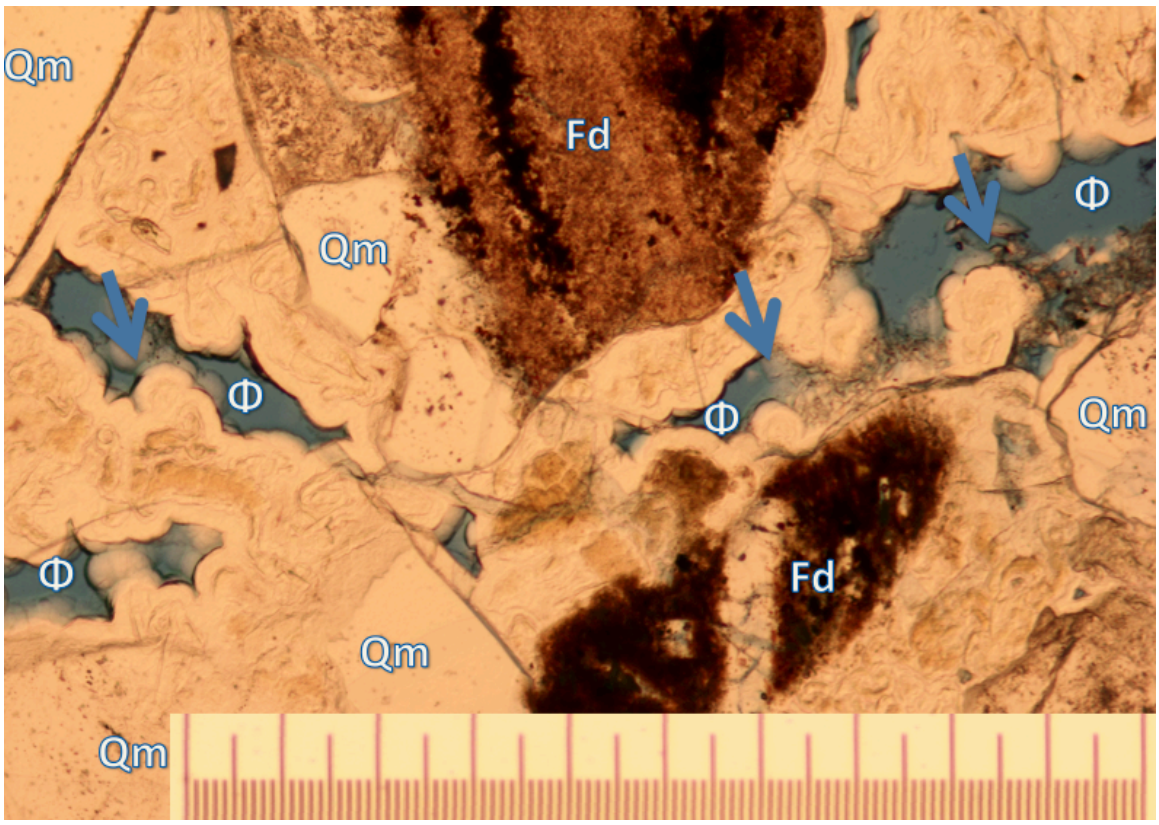

Figure 2 - Polarized photomicrograph of sample LBF_0212_1B with 16x magnification. With further magnification, the opal cement is more defined and seen nucleating from framework grains filling intergranular porosity. Scale bar is 1mm.

Thin sections were made from unconsolidated, laminated sand located on the footwall side of the fault to provide a basis for depositional system. Sample LBF_FWSED1 (Figure 3) was taken adjacent to the area where the fault exhibits discontinuous concretionary cementation and LBF_FWSED2 (Figure 4) was taken 300m perpendicular to the strike of the fully cemented section. Microscopy performed on LBF_FWSED1 revealed relatively immature sand with monocrystalline quartz, unaltered feldspars, phyllosillicates identified as biotite, and laminations of opaque heavy minerals identified as magnetite. Magnetite laminations are interpreted as overbank deposits where heavy minerals where hydraulically sorted to represent the bottom of the depositional event. Sample LBF_FWSED2 was also identified as a relatively immature sand with similar framework grains. The primary difference identified was the distribution of heavy minerals within the thin section and presence of clay rims on the grains. The sample is weakly laminated and heavy minerals make up only 5% of the thin section as opposed to LBF_FWSED1 in which heavy minerals make up 30% of the thin section.

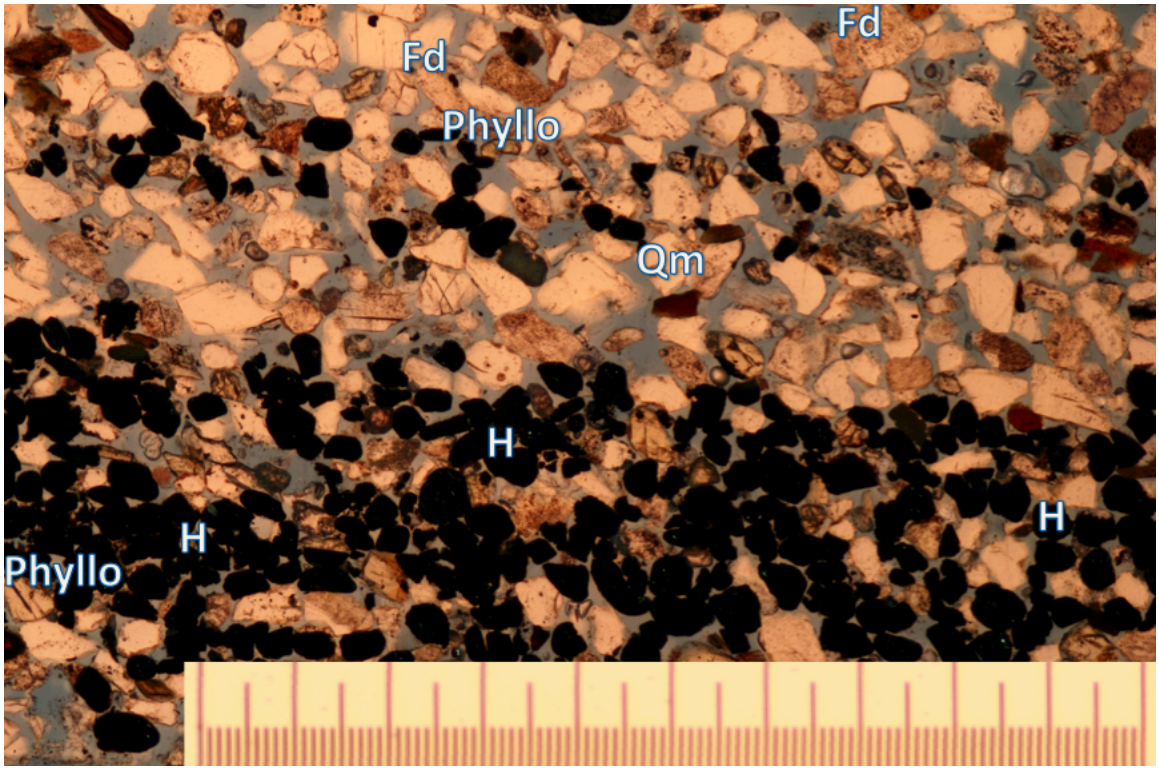

Figure 3 - Polarized photomicrograph of sample LBF_FWSED1 with 16x magnification. The sample is perpendicular to bedding and is oriented with up being the top of the photo. Monocrystalline quartz grains are angular to sub-angular with the addition of intact, unaltered feldspars and phyllosillicates indicating an immature sand. Sample shows no noticeable cementation in intergranular pore space. Scale bar is 1mm.

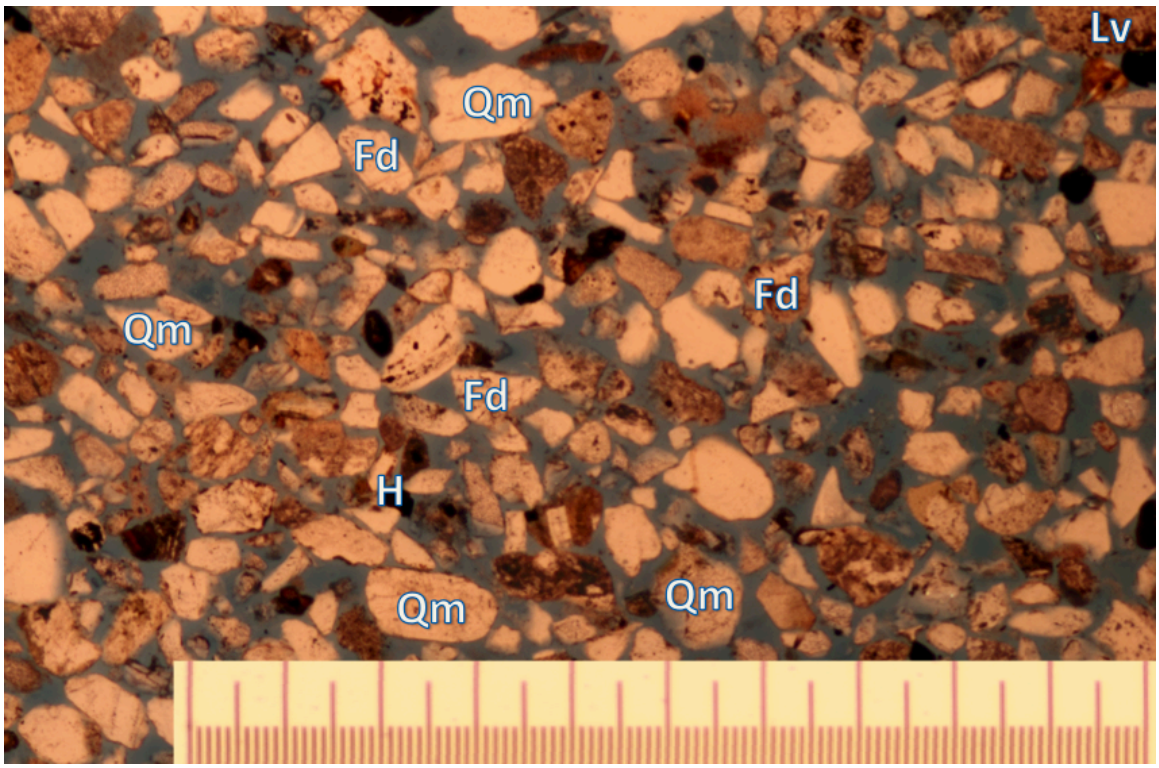

Figure 4 - Polarized photomicrograph of sample LBF_FWSED2 with 16x magnification. The sample is perpendicular to weak bedding observed in outcrop and is oriented with up being the top of the photo. The sand is compositionally similar to LBF_FWSED1 with differences in heavy mineral distribution. LBF_FWSED2 also exhibits slightly more intergranular pore space indicated by blue epoxy. Scale bar is 1mm.

Porosimetry analysis targeted morphologically distinct sections of the fault with regards to overall cementation, and results indicate noticeable differences in the overall calculated porosity and permeability. Samples LBF_HW1 and LBF_FW1 were collected from the hanging wall and footwall of the completely cemented fault core. These two samples demonstrate strong measured differences in their calculated porosity and permeability. Sample LBF_HW1 (Hanging wall) has a measured porosity of 13.06% and permeability of 21.86md. Sample LBF_FW1 (Footwall) has a measured porosity of 3.3% and permeability of 0.01md. These two samples were taken at the fully cemented section of the fault. Sample LBF_HW2 (Hanging wall) has a measured porosity of 8.69% and permeability of 1.08md. Sample LBF_FW2 (Footwall) has a measured porosity of 7.1% and permeability of 0.98md. These two samples were taken at the partially cemented section of the fault. These values are represented on a permeability versus porosity cross plot seen in Figure 5. Full tables of MIP data are included in the Appendix.

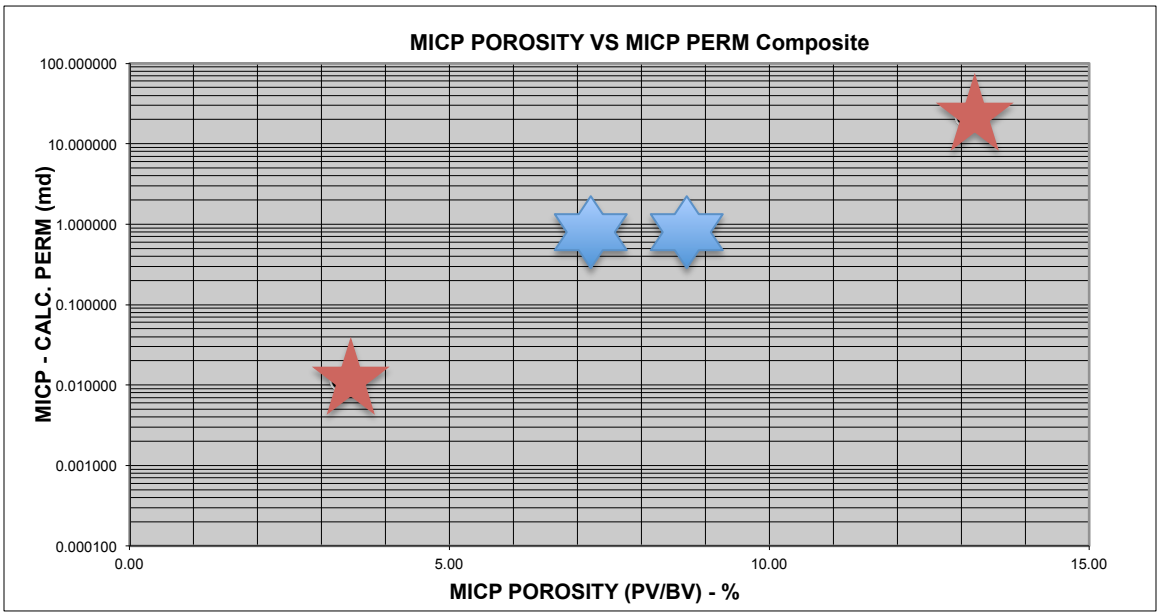

- Fully cemented section

- Partially cemented section

Figure 5 – Cross plot of calculated mercury intrusion permeability in millidarcies and porosity in porosity volume as a percentage of bulk volume. Porosity and permeability values for the partially cemented section of the fault show similarities whereas values for the fully cemented section show noticeable differences between the footwall and hanging wall samples.

DISCUSSION

Petrography performed on the thin sections indicates that the unconsolidated, laminated sand found in outcrop on the footwall side of Loma Blanca fault was deposited in a fluvial environment. Possible depositional systems include ancestral feeders into the Rio Salado and overbank facies. Overbank facies depositional environment is inferred by laminations of heavy minerals that were preferentially hydraulically sorted due to their higher specific gravity. In a fluvial system with sufficient energy to initiate transport, the magnetite grains would sort to the bottom of the sediment transport column. The clay coating observed on grains in thin section LBF_FWSED2 build on the fluvial deposition hypothesis with the possibility of marine based biofilms contributing to clay development (Woolridge et. al 2017). Identifying depositional systems for the uppermost sand is essential for developing the hydrostratigraphic model. The model will provide the basis for future numerical analysis. Discovery of opal cement in samples LBF_0212_1A and LBF_0212_1B fundamentally changes the understanding of diagenesis surrounding the Loma Blanca fault damage zone. The original hypothesis stated the primary cementation component as calcium carbonate; future research will attempt to reconcile the presence of silica-based cement. The opal cement may have been sourced internally from pressure solution (Bjorlykke and Egeberg, 1993), however a sufficient heat source would be needed to elevate fluid temperatures above the threshold for silica saturation. This poses another question regarding the subsurface fluid flow history of the fault and whether deep basinal fluids were

introduced into the system as well as native groundwater moving down gradient within the zone of saturation.

Porosimetry data indicates that changes in cementation style produce distinct porosity and permeability characteristics. Sample LBF_HW1 produced median pore diameters for volume and area of 2.41μm and 0.012μm respectively while sample LBF_FW1 produced median pore diameters for volume and area of 0.3μm and 0.07μm respectively. The difference in the median pore volume between the footwall and the hanging wall is an 800% increase in the fully cemented section of the fault whereas the median pore volume for the partially cemented section data fell within a much closer range. Sample LBF_HW2 produced median pore diameters for volume and area of 1.32μm and 0.008μm respectively while sample LBF_FW2 produced median pore diameters for volume and area of 1.64μm and 0.02μm respectively. Initial first order observations taking into account calculated porosity and permeability as well as median pore volume and area indicate lateral lithologic and grain size heterogeneity along fault strike contributing to overall fault cementation. This observation is corroborated by the morphological and compositional differences seen in thin sections taken from unconsolidated sediment on the footwall side of the fault. Surficial data and observations are currently being incorporated with subsurface data obtained through coring operations and installation of pump and monitoring wells.

FUTURE WORK

Three directional boreholes and 4 monitoring wells, two on either side of the fault, were drilled between the months of May and July 2017 (Figure 6). The directional wells were drilled at 45˚ in order to intersect the fault at depth. Drilling was performed by a sonic rig and recovered core throughout the 113 ft borehole. Additional subsurface samples were taken every 5 ft while drilling monitoring wells. Cross sections and fence diagrams will be constructed to ascertain stratigraphy on the northern end of the fault closest to the Rio Salado. Core and grain size analysis will provide a detailed framework for building a 3-dimensional subsurface model by obtaining quantitative porosity and permeability data. The model will be constructed in the Leapfrog software package and create grids to use in hydrogeologic numerical analysis for flow simulation. Additionally, the subsurface model will influence the location of an additional 20 pump and monitoring wells to be installed in the coming year for cross-fault pump tests. Measured sections on either side of the fault will correlate outcrop stratigraphy and subsequently be incorporated into the model as additional lithologic, grain size, and permeability data. Additionally, XRD analysis is scheduled for silt and clay fractions encountered at approximately 75 ft in depth. Resulting elemental signatures will compare against upper to mid Miocene silts and clay that compose playa bed facies on the footwall of the Loma Pelada fault located approximately half a mile to the west of the Loma Blanca fault. Relating the silt and clay units should provide a better constraint on the throw of the fault and provide insight on the effects on the possible confining silt and clay unit in relation to local hydrogeology.

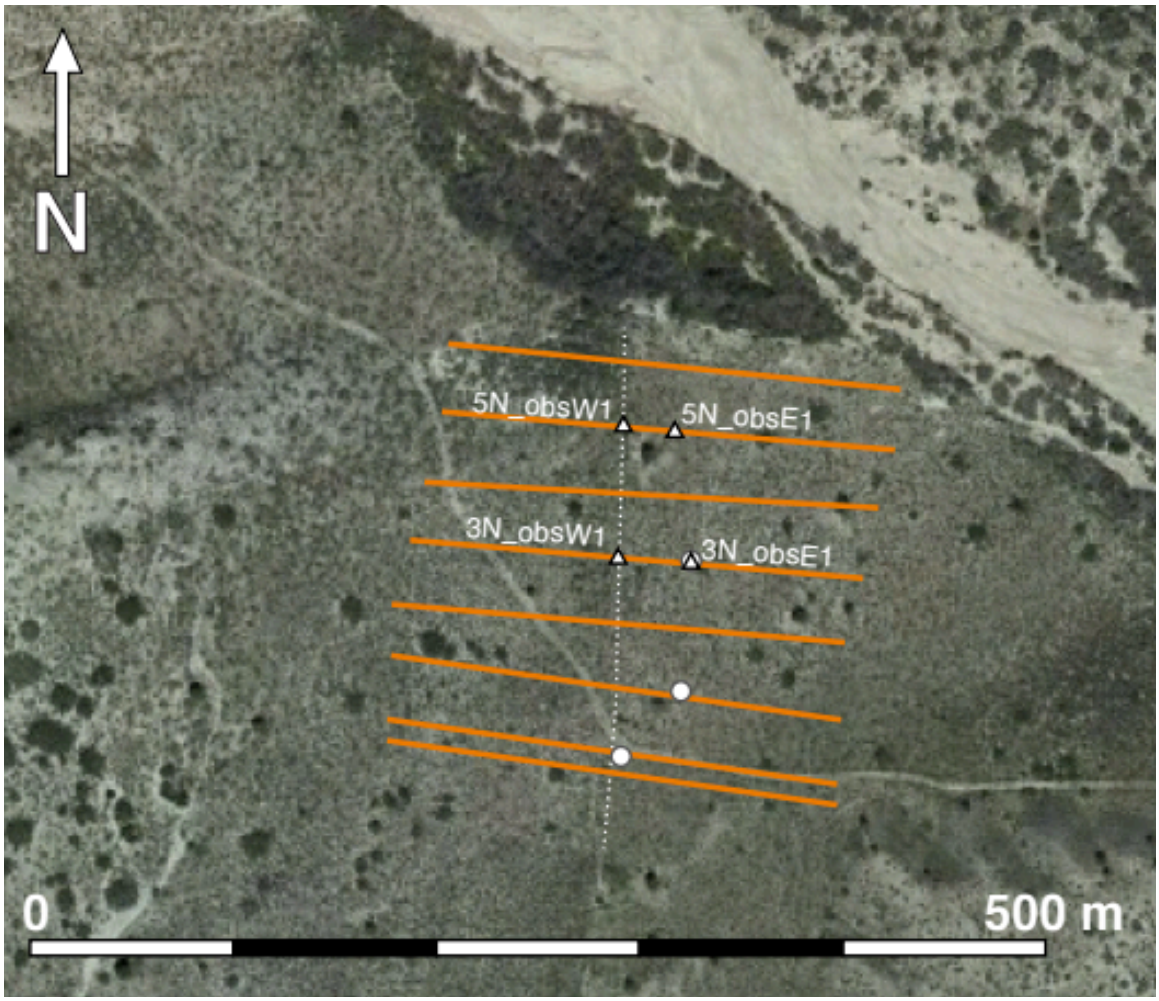

Figure 6 – Satellite imagery of the north end of the Loma Blanca fault. The dotted line represents the fault, orange lines represent geophysical resistivity transects perpendicular to the fault, circles represent location of directional boreholes drilled west to intersect the fault with core recovery, and triangles represent location of monitoring wells.

REFERENCES

Bretan, P., G. Yielding, and H. Jones (2003), Using calibrated shale gouge ratio to estimate hydrocarbon column heights, *Aapg Bulletin*, *87*(3), 397-413, doi:10.1306/08010201128.

Bjorlykke, Knut, and P. K. Egeberg. "Quartz cementation in sedimentary basins." *AAPG bulletin* 77.9 (1993): 1538-1548.

Catalan, Lionel, et al. "An experimental study of secondary oil migration (1)." *AAPG Bulletin* 76.5 (1992): 638-650.

Childs, C., Ø. Sylta, S. Moriya, J. J. Walsh, and T. Manzocchi (2002), A method for including the capillary properties of faults in hydrocarbon migration models, in *Norwegian Petroleum Society Special Publications*, edited by G. K. Andreas and H. Robert, pp. 127-139, Elsevier, doi:http://dx.doi.org/10.1016/S0928-8937(02)80011-X.

Dewhurst, David N., Richard M. Jones, and Mark D. Raven. "Microstructural and petrophysical characterization of Muderong Shale: application to top seal risking." *Petroleum Geoscience* 8.4 (2002): 371-383.

Dickinson, W.R., 1970. Interpreting detrital modes of graywacke and arkose. Journal of Sedimentary Petrology 40, 695-707.

Folk, R.L., 1980. Petrology of sedimentary rocks. Hemphill Publ. Co., Austin, TX, Austin, TX, United States (USA), 184 pp.

Fristad, T., A. Groth, G. Yielding, and B. Freeman (1997), Quantitative fault seal prediction: a case study from Oseberg Syd, in *Norwegian Petroleum Society Special Publications*, edited by P. Møller-Pedersen and A. G. Koestler, pp. 107-124, Elsevier, doi:http://dx.doi.org/10.1016/S0928-8937(97)80010-0.

Fulljames, J. R., L. J. J. Zijerveld, and R. C. M. W. Franssen (1997), Fault seal processes: systematic analysis of fault seals over geological and production time scales, in *Norwegian Petroleum Society Special Publications*, edited by P. Møller-Pedersen and A. G. Koestler, pp. 51-59, Elsevier, doi:http://dx.doi.org/10.1016/S0928-8937(97)80006-9.

Ingersoll, R.V., Suczek, C.A., 1979. Petrology and provenance of Neogene sand from Nicobar and Bengal fans, DSDP sites 211 and 218. Journal of Sedimentary Petrology 49, 1217-1228.

Katz, A. J., and A. H. Thompson. "Prediction of rock electrical conductivity from mercury injection measurements." *Journal of Geophysical Research: Solid Earth* 92.B1 (1987): 599-607.

Lindsay, N. G., F. C. Murphy, J. J. Walsh, and J. Watterson (1993), Outcrop Studies of Shale Smears on Fault Surface, in *The Geological Modelling of Hydrocarbon Reservoirs and Outcrop Analogues*, edited, pp. 113-123, Blackwell Publishing Ltd., doi:10.1002/9781444303957.ch6.

Manzocchi, T., C. Childs, and J. J. Walsh (2010), Faults and fault properties in hydrocarbon flow models, *Geofluids*, *10*, 94-113.

Welbon, A. I., A. Beach, P. J. Brockbank, O. Fjeld, S. D. Knott, T. Pedersen, and S. Thomas (1997), Fault seal analysis in hydrocarbon exploration and appraisal: examples from offshore mid-Norway, in *Norwegian Petroleum Society Special Publications*, edited by P. Møller-Pedersen and A. G. Koestler, pp. 125-138, Elsevier, doi:http://dx.doi.org/10.1016/S0928-8937(97)80011-2.

Wooldridge, L. J., R. H. Worden, J. Griffiths, A. Thompson, and P. Chung. "Biofilm origin of clay-coated sand grains." *Geology* (2017).

Yielding, G. (2002), Shale Gouge Ratio — calibration by geohistory, in *Norwegian Petroleum Society Special Publications*, edited by G. K. Andreas and H. Robert, pp. 1-15, Elsevier, doi:http://dx.doi.org/10.1016/S0928-8937(02)80003-0.

APPENDIX

Appendix 1 – Photomicrographs

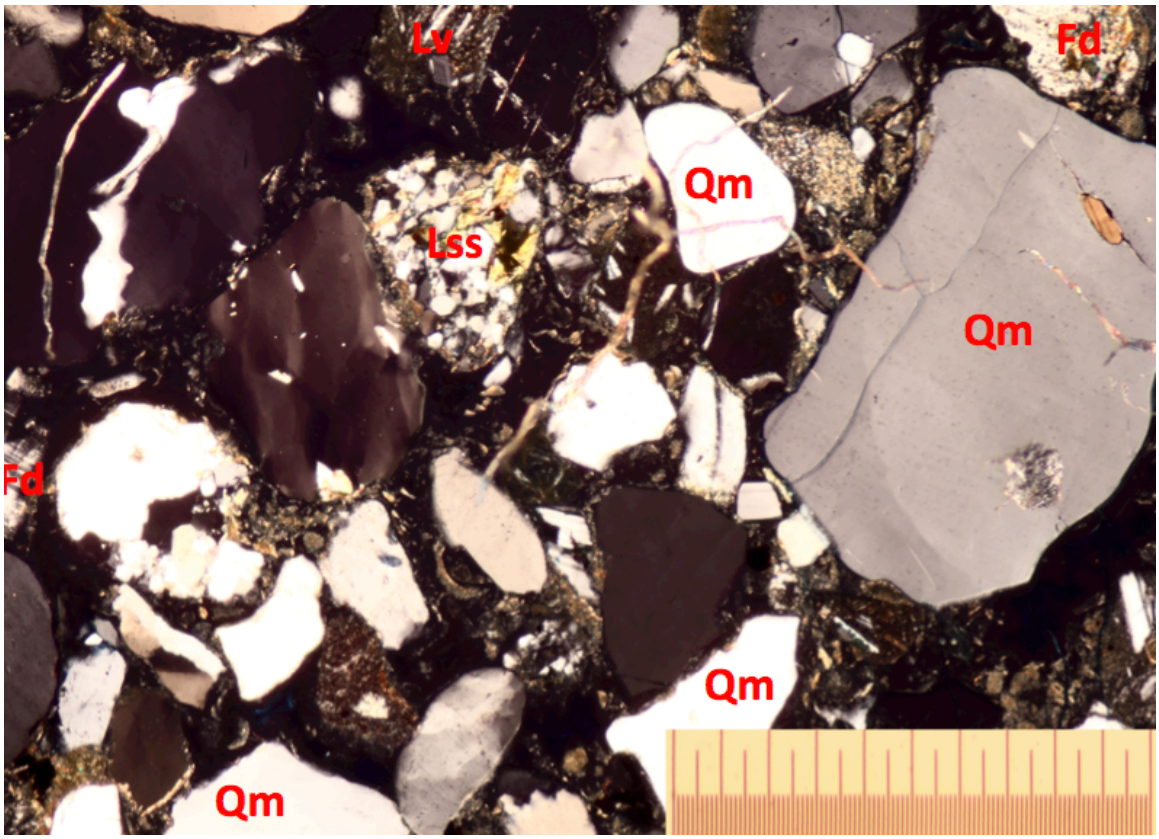

Sample LBF_0212_1A under cross-polarized light and 8x magnification. Opal appears opaque/black in the image. Scale bar is 1mm.

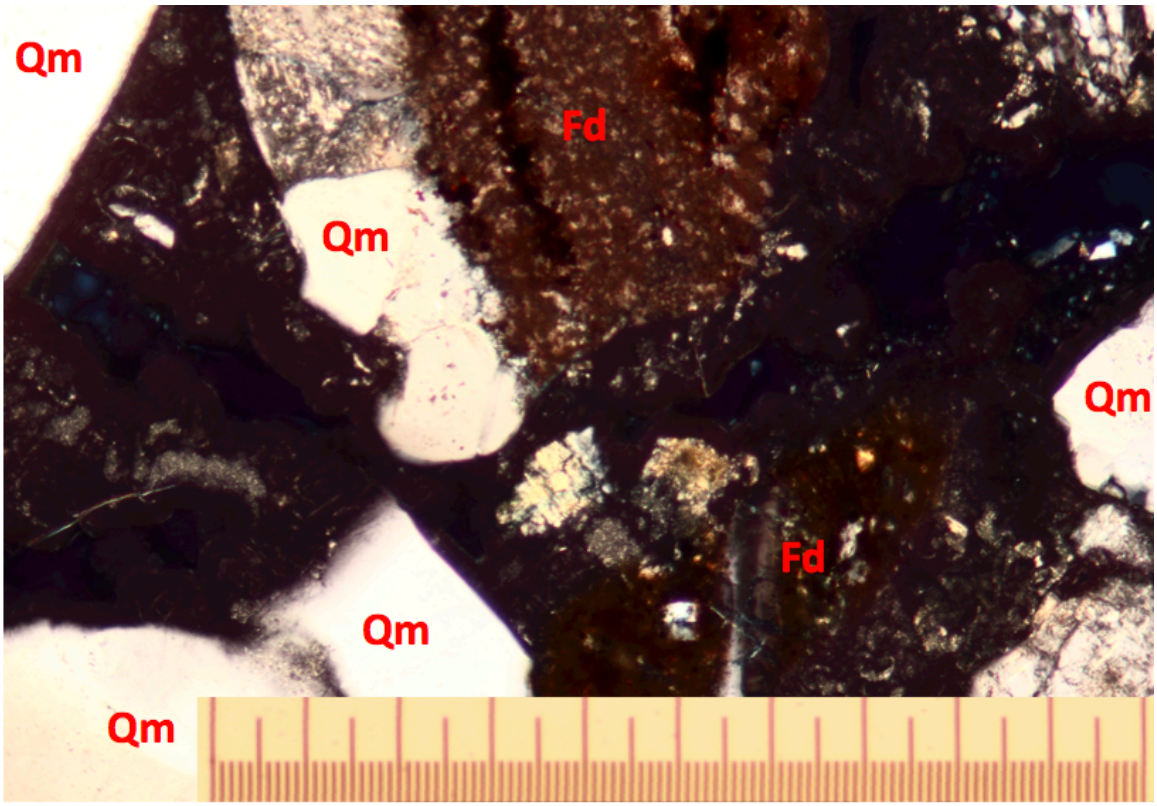

Sample LBF_0212_1B under cross-polarized light and 16x magnification. Opal appears opaque/black in the image. Scale bar is 1mm.

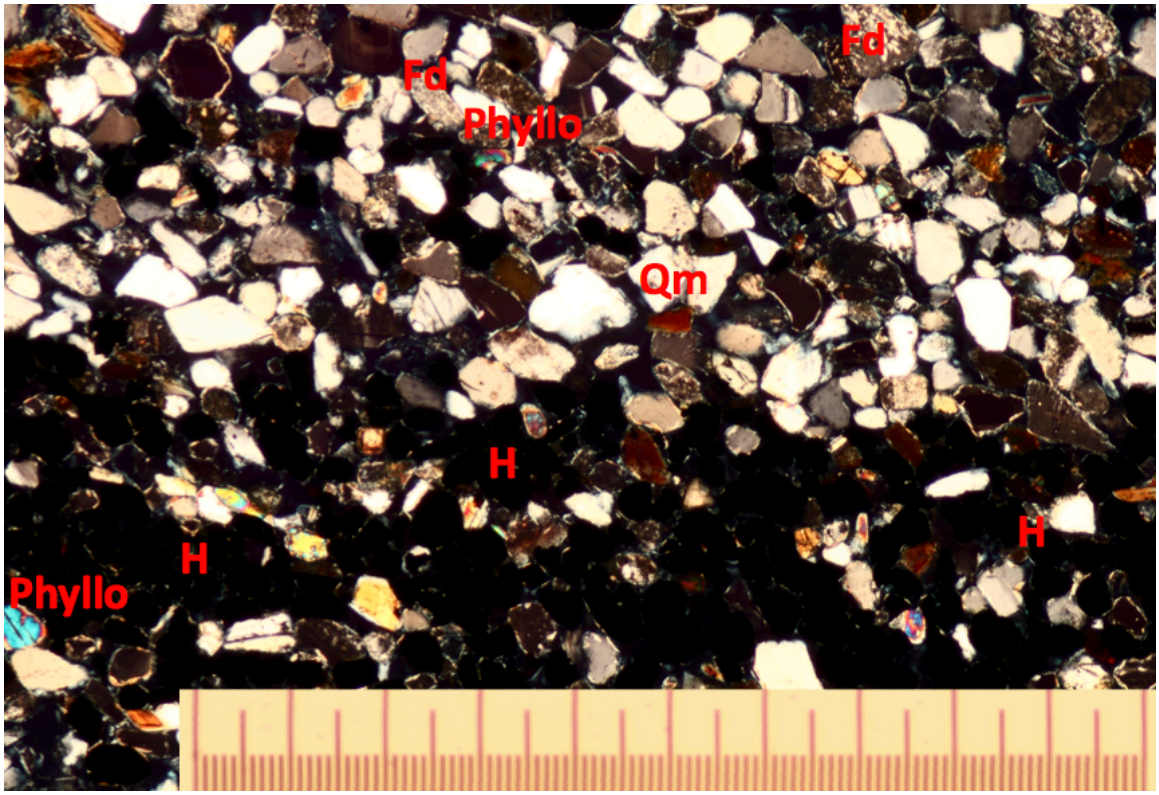

Sample LBF_FWSED1 under cross-polarized light and 16x magnification. Horizontal lamination of opaque minerals identified as magnetite. Oriented so that the photomicrograph is perpendicular to bedding and top is up-section. Scale bar is 1mm.

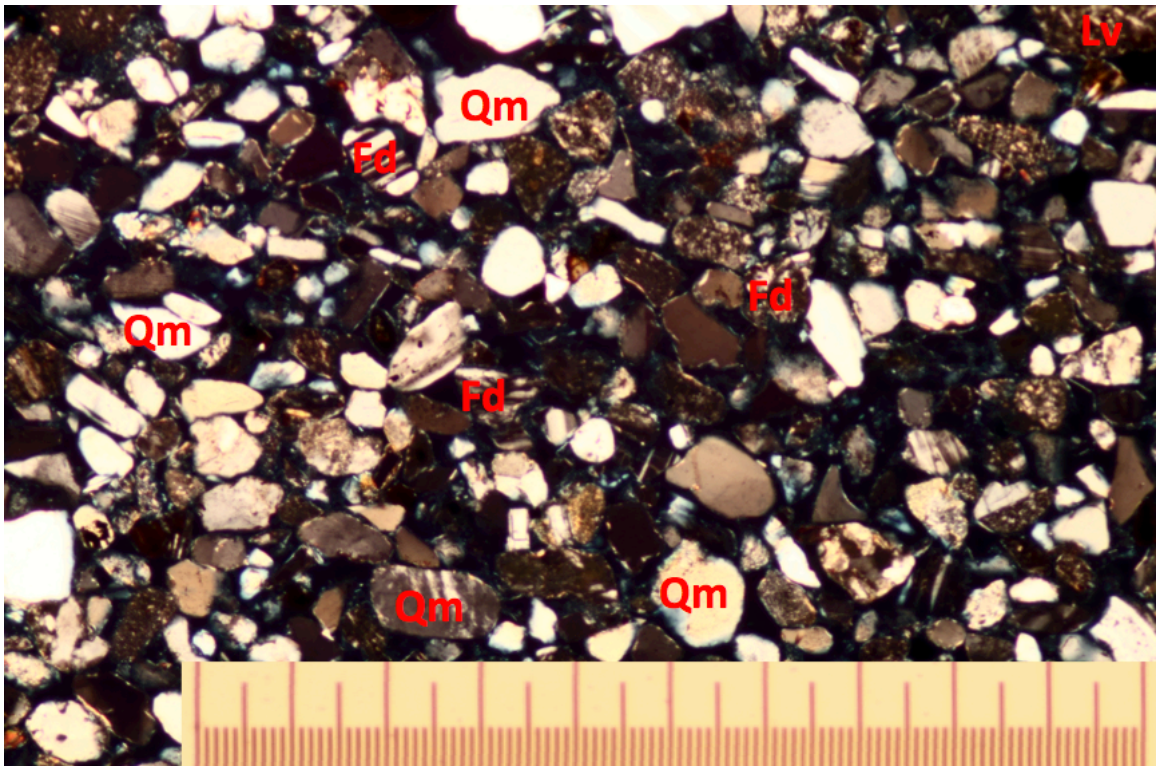

Sample LBF_FWSED2 under cross-polarized light and 16x magnification. Oriented so that the photomicrograph is perpendicular to bedding and top is up-section. Scale bar is 1mm.

Appendix 2 – Mercury intrusion porosimetry data

LBF_HW1

Total I Intrusion Volume =	0.0564	mL/g
Total Pore Area =	1.39	m²/g
Median Pore Diameter (Volume) =	2.4181	µm
Median Pore Diameter (Area) =	0.012	µm
Average Pore Diameter (4V/A) =	0.1622	µm
Bulk Density at 4.40 psia =	2.3162	g/mL
Apparent (skeletal) Density =	2.6641	g/mL
Porosity =	13.0618	%
Stem Volume Used =	66	%

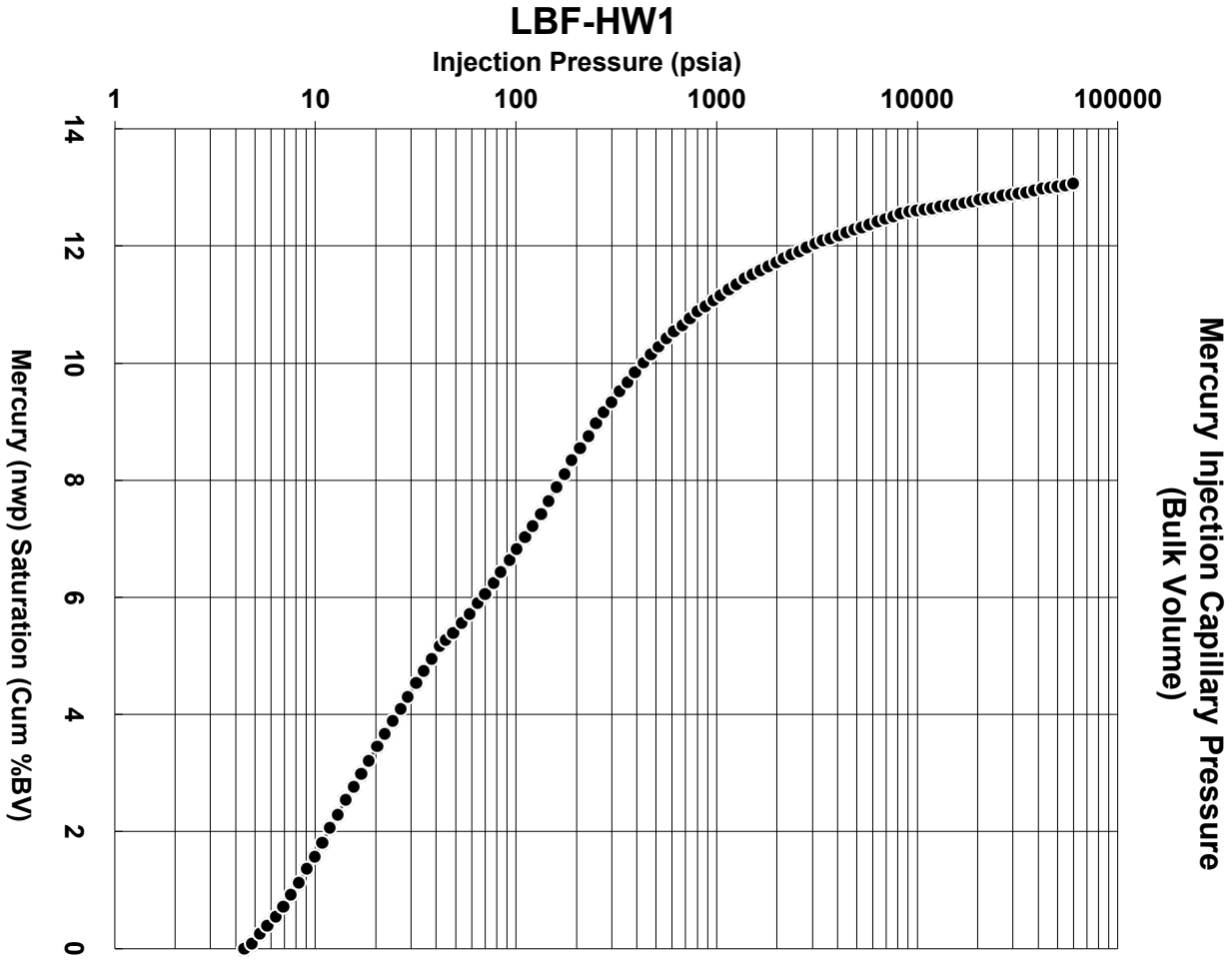

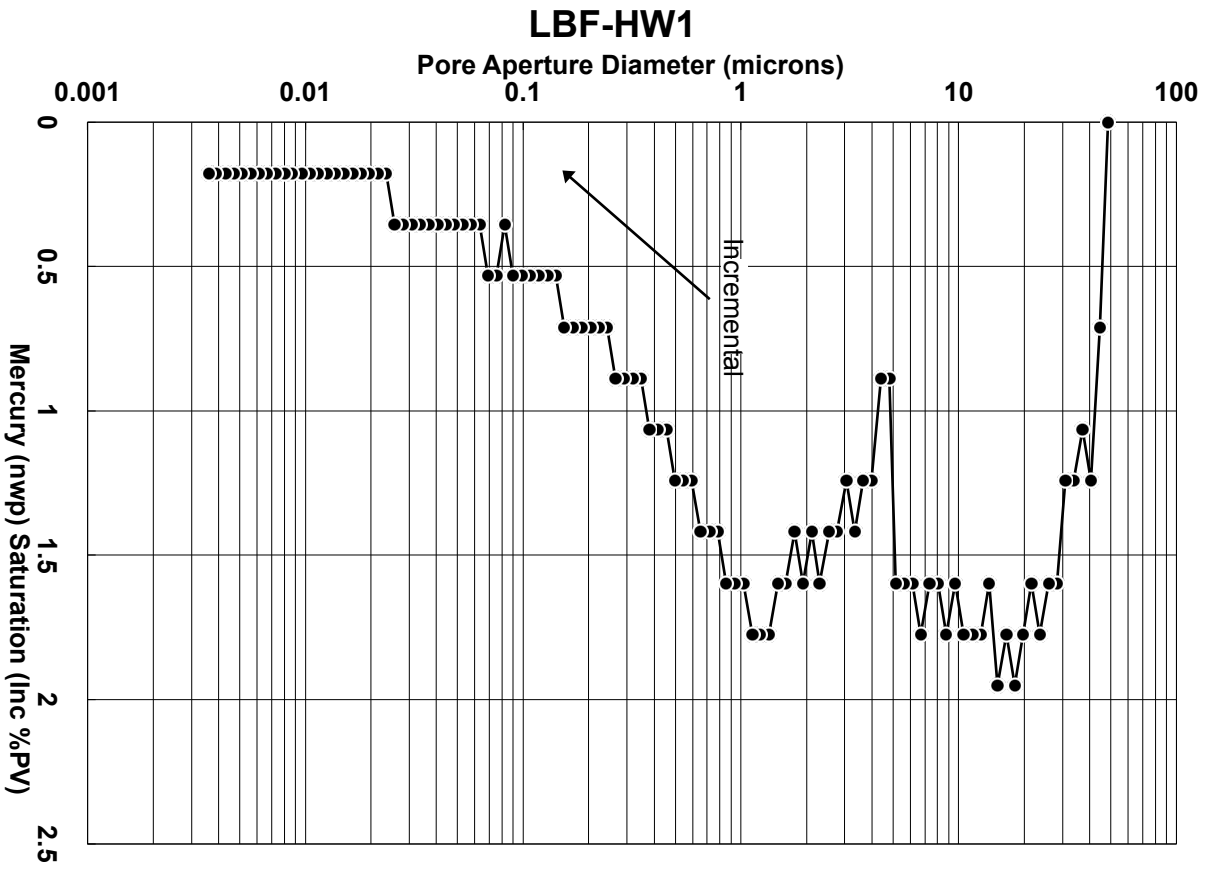
LBF-HW1
Pore Aperture Diameter (microns)
0.001
0.01
0.1
1
10
100
0
0.5
1
1.5
2
2.5
Mercury (nwp) Saturation (Inc %PV)
Incremental

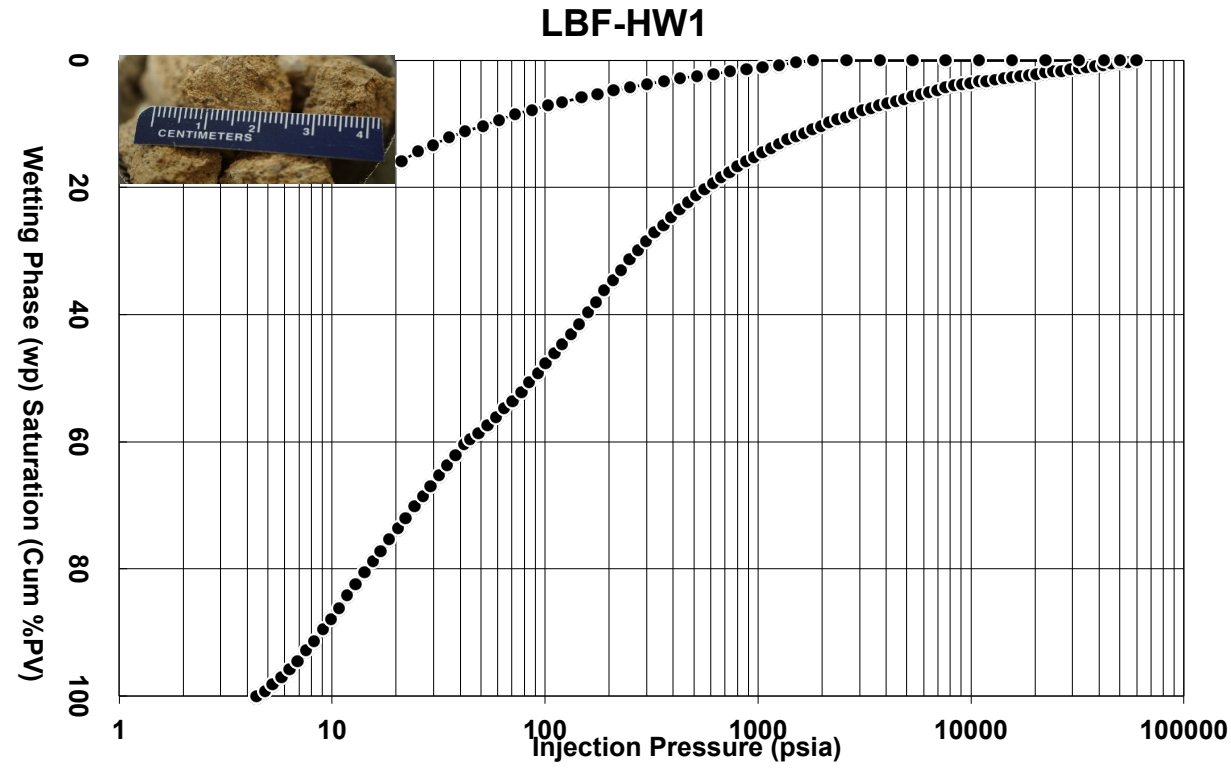
LBF-HW1
CENTIMETERS
0
20
40
60
80
100
Wetting Phase (wp) Saturation (Cum %PV)
1
10
100
1000
10000
100000
Injection Pressure (psia)

LBF_HW2

Total I Intrusion Volume =	0.0369	mL/g
Total Pore Area =	1.601	m²/g
Median Pore Diameter (Volume) =	1.3299	µm
Median Pore Diameter (Area) =	0.0083	µm
Average Pore Diameter (4V/A) =	0.0921	µm
Bulk Density at 4.40 psia =	2.4459	g/mL
Apparent (skeletal) Density =	2.6883	g/mL
Porosity =	9.0166	%
Stem Volume Used =	28	%

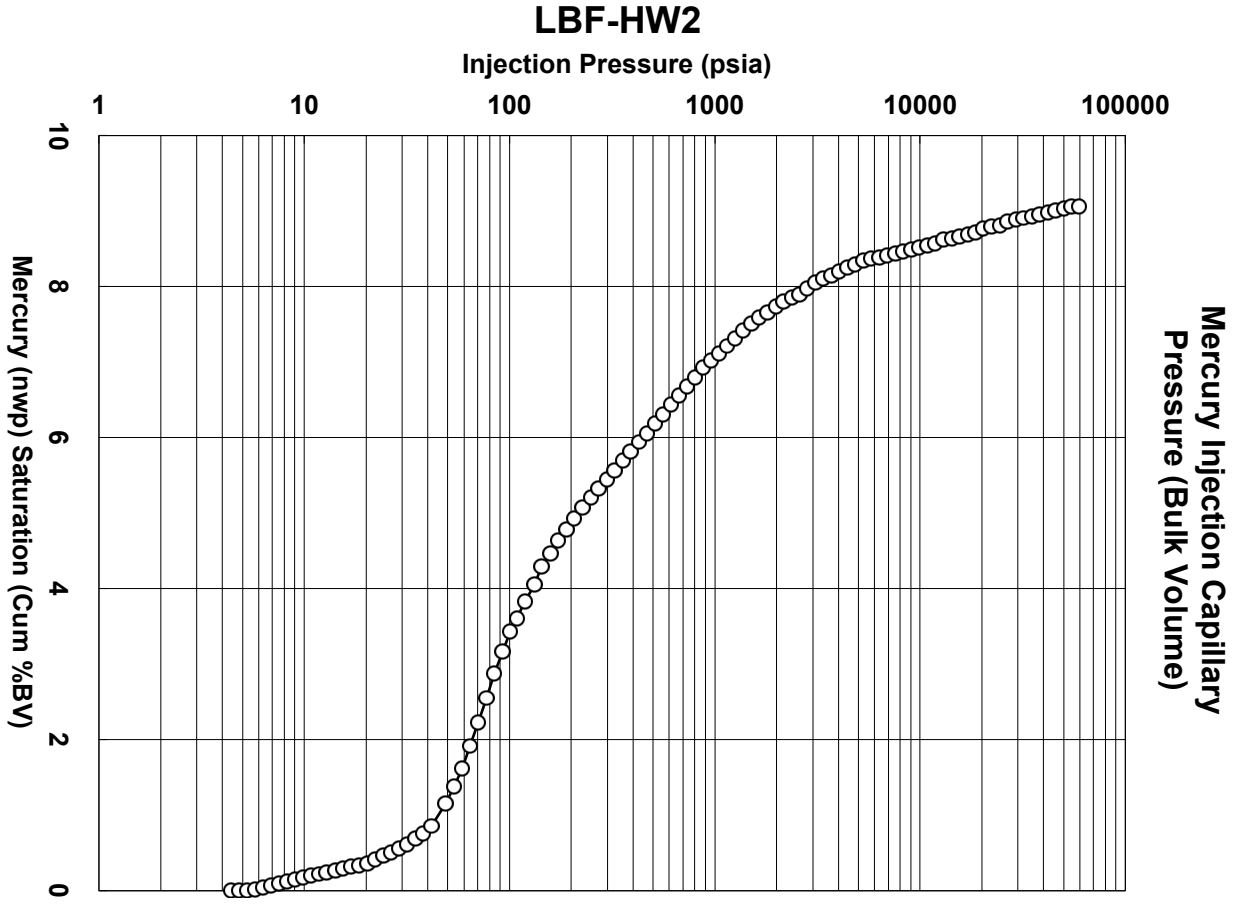

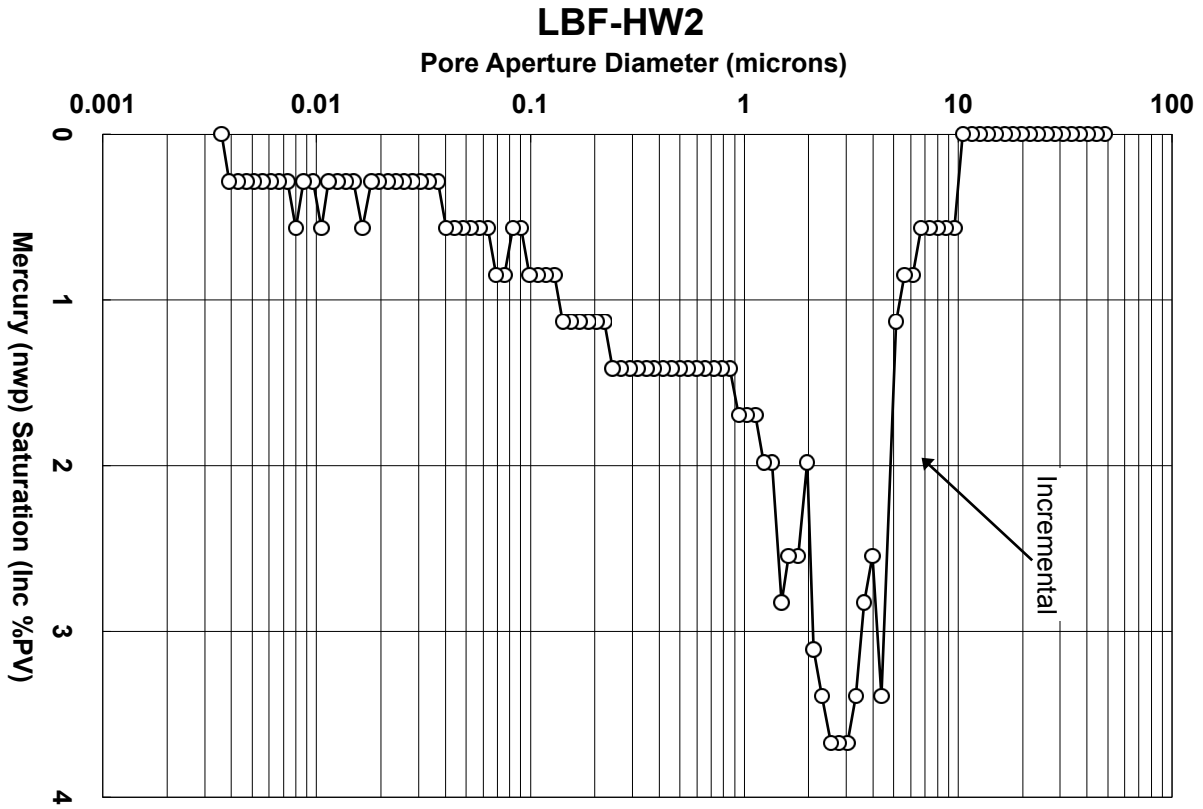
LBF-HW2
Pore Aperture Diameter (microns)
0.001
0.01
0.1
1
10
100
Mercury (nwp) Saturation (Inc %PV)
0
1
2
3
4
Incremental

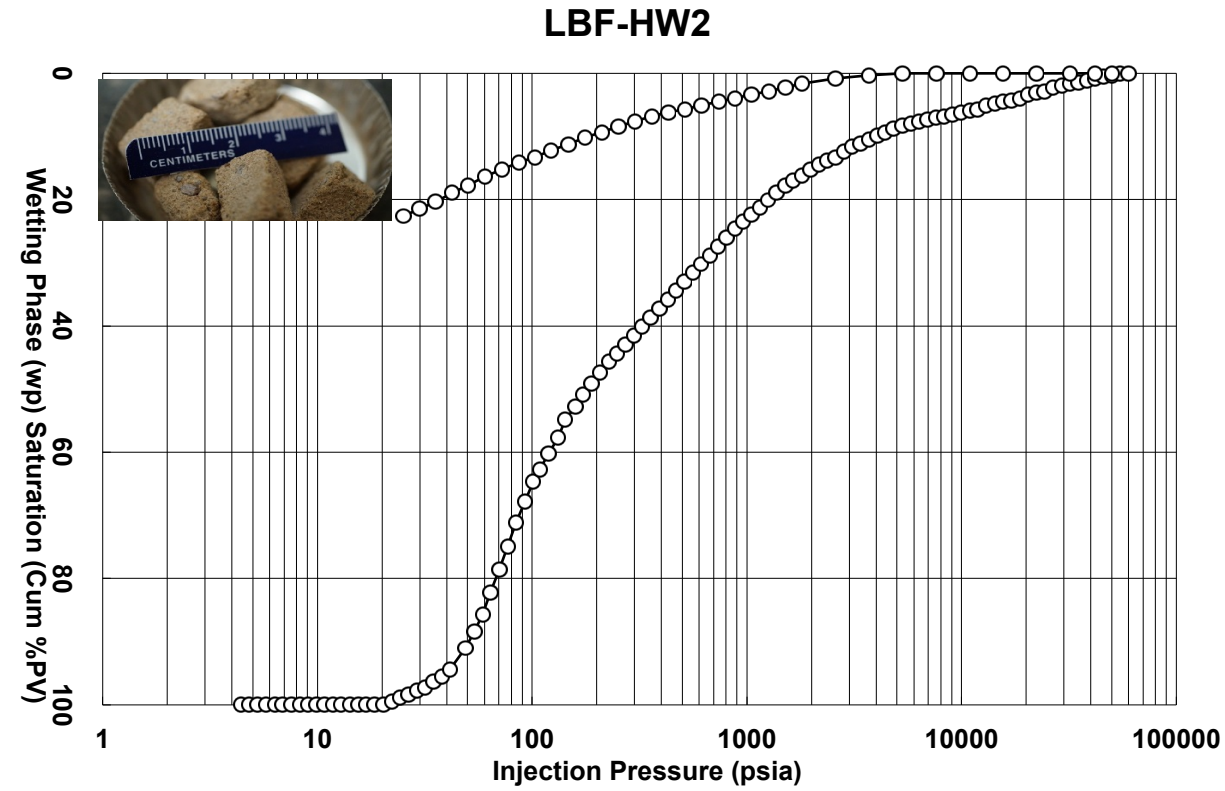
LBF-HW2
Wetting Phase (wp) Saturation (Cum %PV)
0
20
40
60
80
100
1
10
100
1000
10000
100000
Injection Pressure (psia)
CENTIMETERS

LBF_FW1

Total I Intrusion Volume =	0.0142	mL/g
Total Pore Area =	0.403	m²/g
Median Pore Diameter (Volume) =	0.3067	µm
Median Pore Diameter (Area) =	0.0707	µm
Average Pore Diameter (4V/A) =	0.1407	µm
Bulk Density at 4.40 psia =	2.5714	g/mL
Apparent (skeletal) Density =	2.6686	g/mL
Porosity =	3.6426	%
Stem Volume Used =	17	% ****

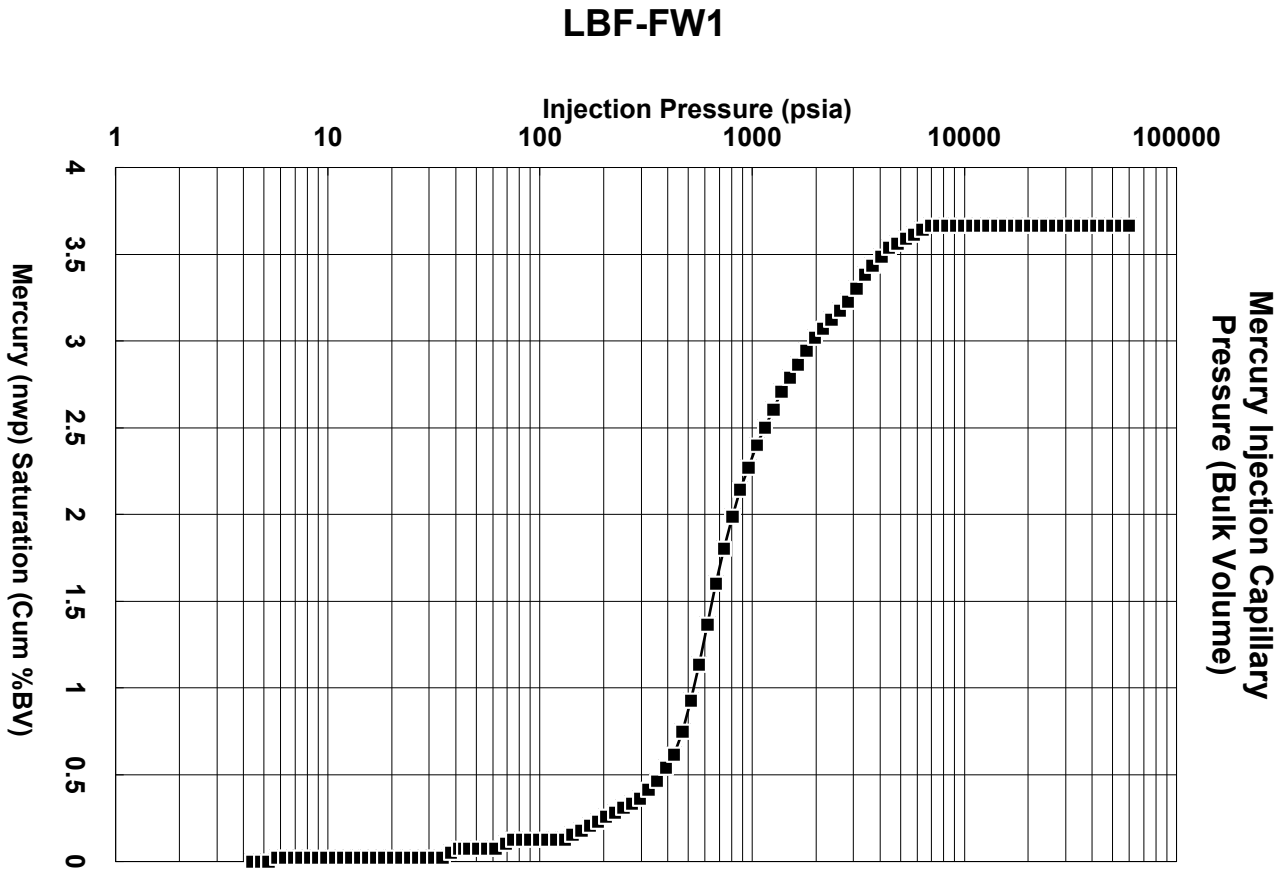

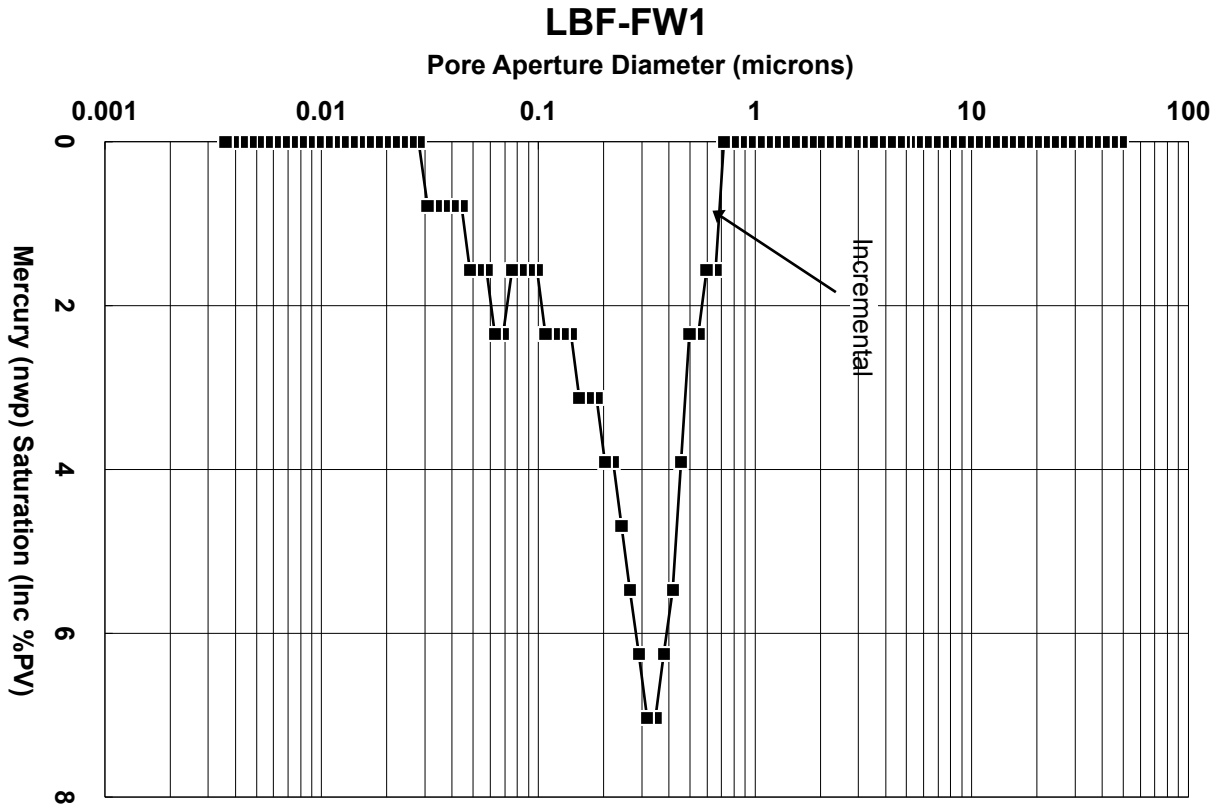
LBF-FW1
Pore Aperture Diameter (microns)
0.001
0.01
0.1
1
10
100
0
2
4
6
8
Mercury (nwp) Saturation (Inc %PV)
Incremental

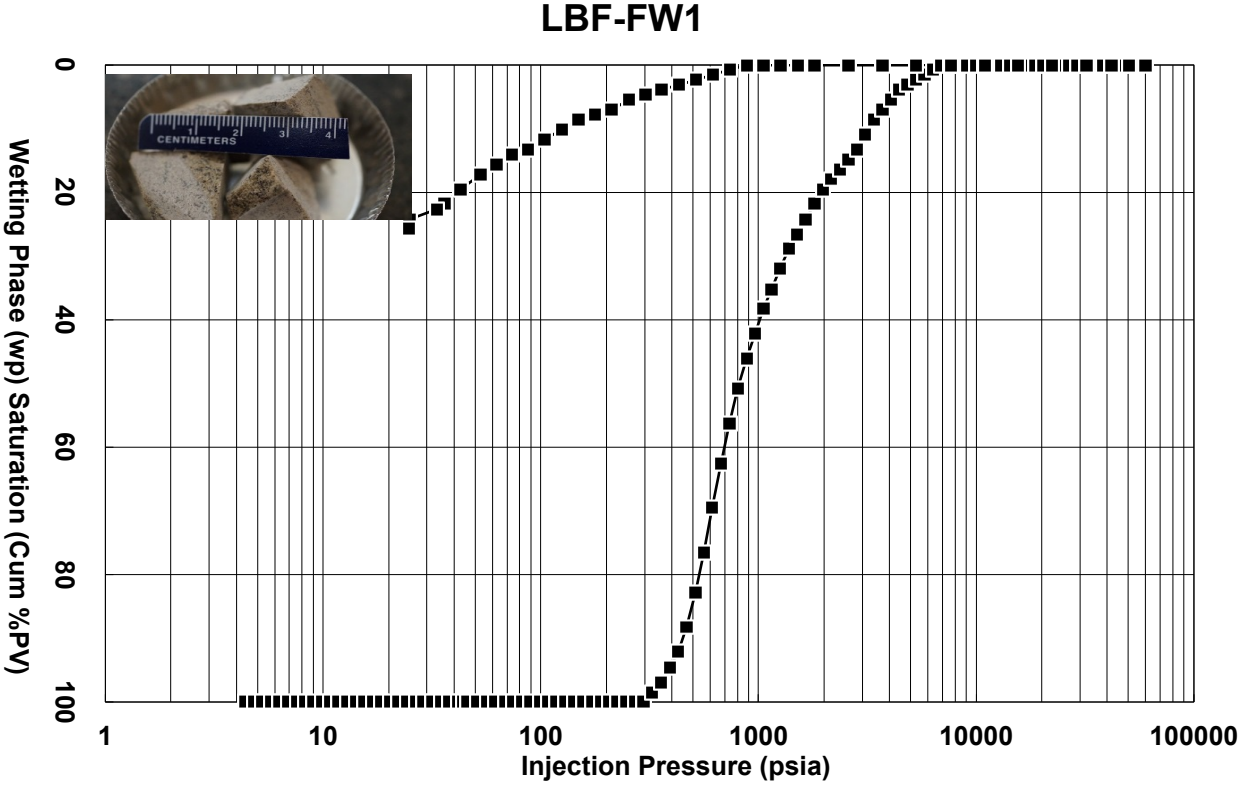
LBF-FW1
0
20
40
60
80
100
Wetting Phase (wp) Saturation (Cum %PV)
CENTIMETERS
1
10
100
1000
10000
100000
Injection Pressure (psia)

LBF_FW2

Total I Intrusion Volume =	0.0306	mL/g
Total Pore Area =	0.61	m²/g
Median Pore Diameter (Volume) =	1.6401	µm
Median Pore Diameter (Area) =	0.021	µm
Average Pore Diameter (4V/A) =	0.2007	µm
Bulk Density at 4.40 psia =	2.4008	g/mL
Apparent (skeletal) Density =	2.5913	g/mL
Porosity =	7.3498	%
Stem Volume Used =	34	%

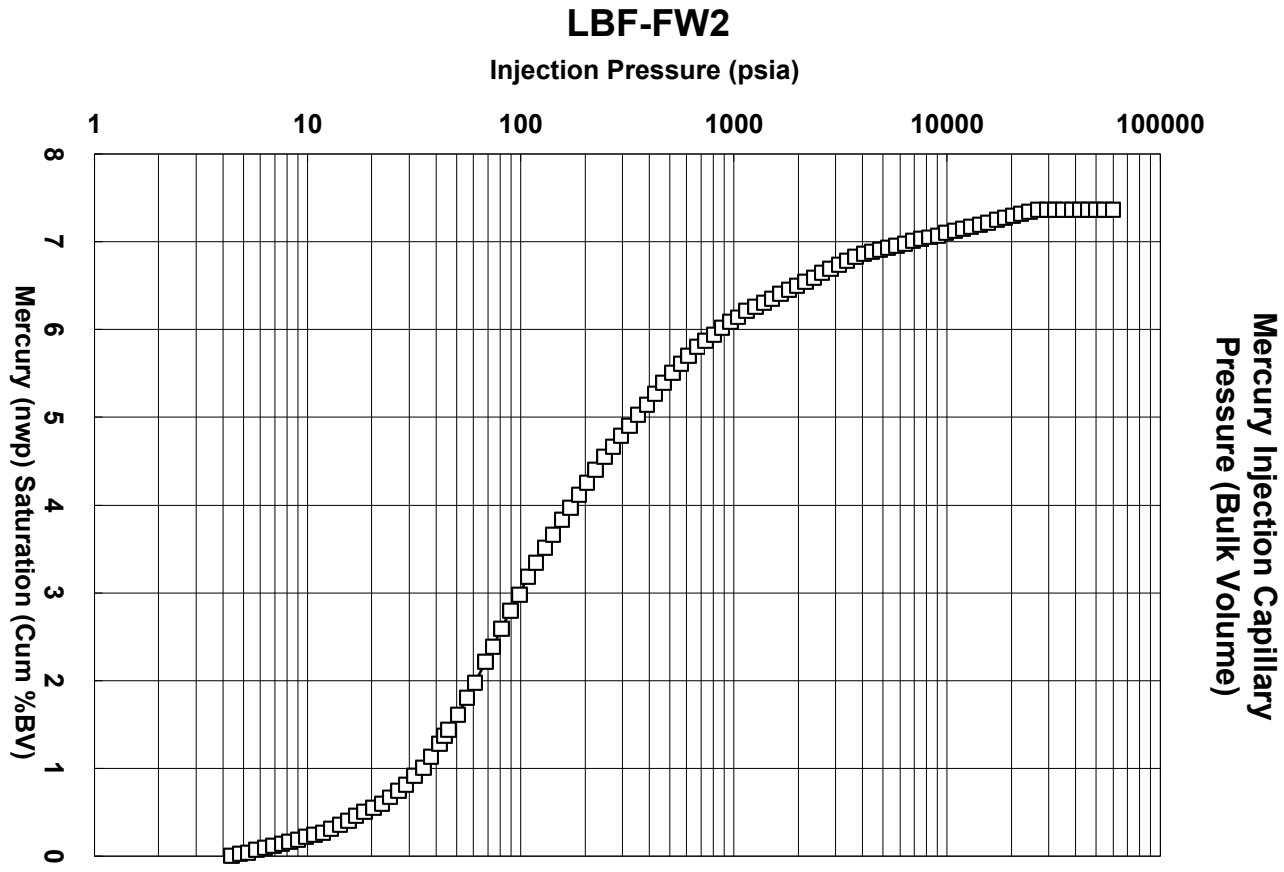

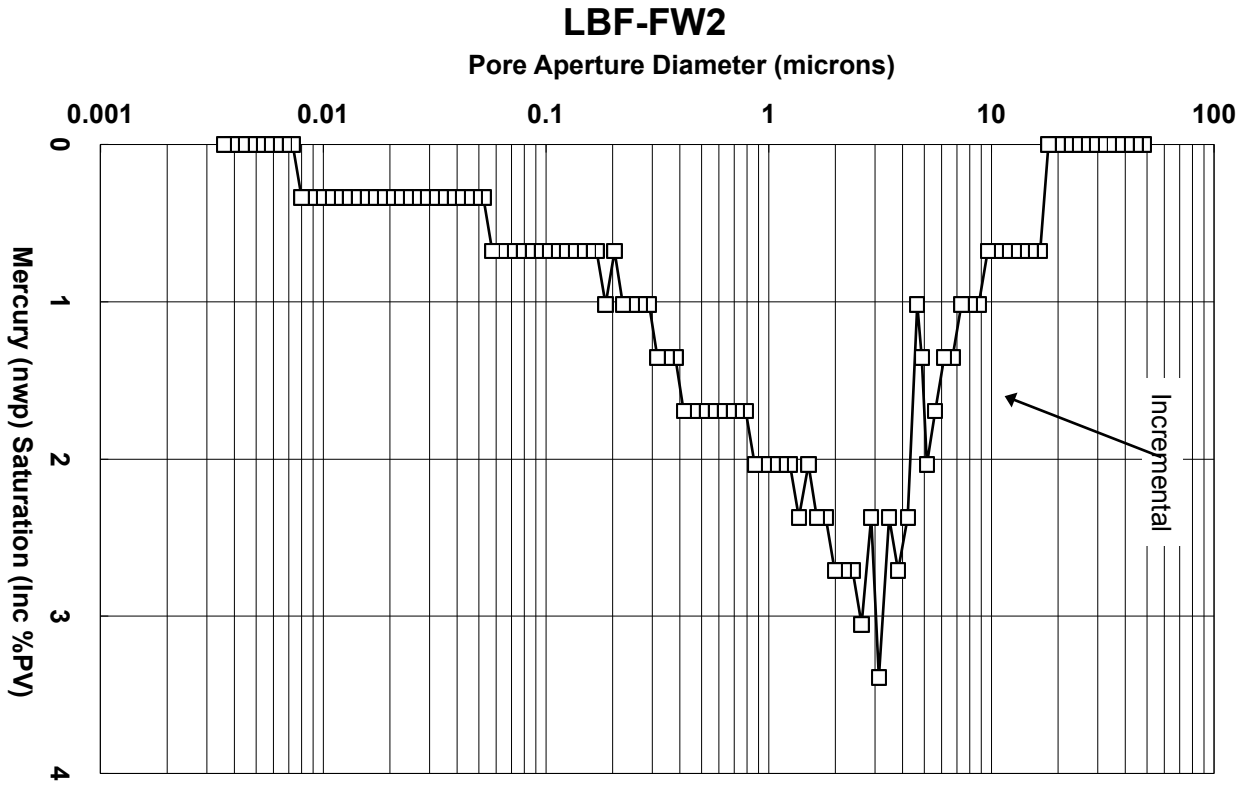
LBF-FW2
Pore Aperture Diameter (microns)
0.001
0.01
0.1
1
10
100
0
1
2
3
4
Mercury (nwp) Saturation (Inc %PV)
Incremental

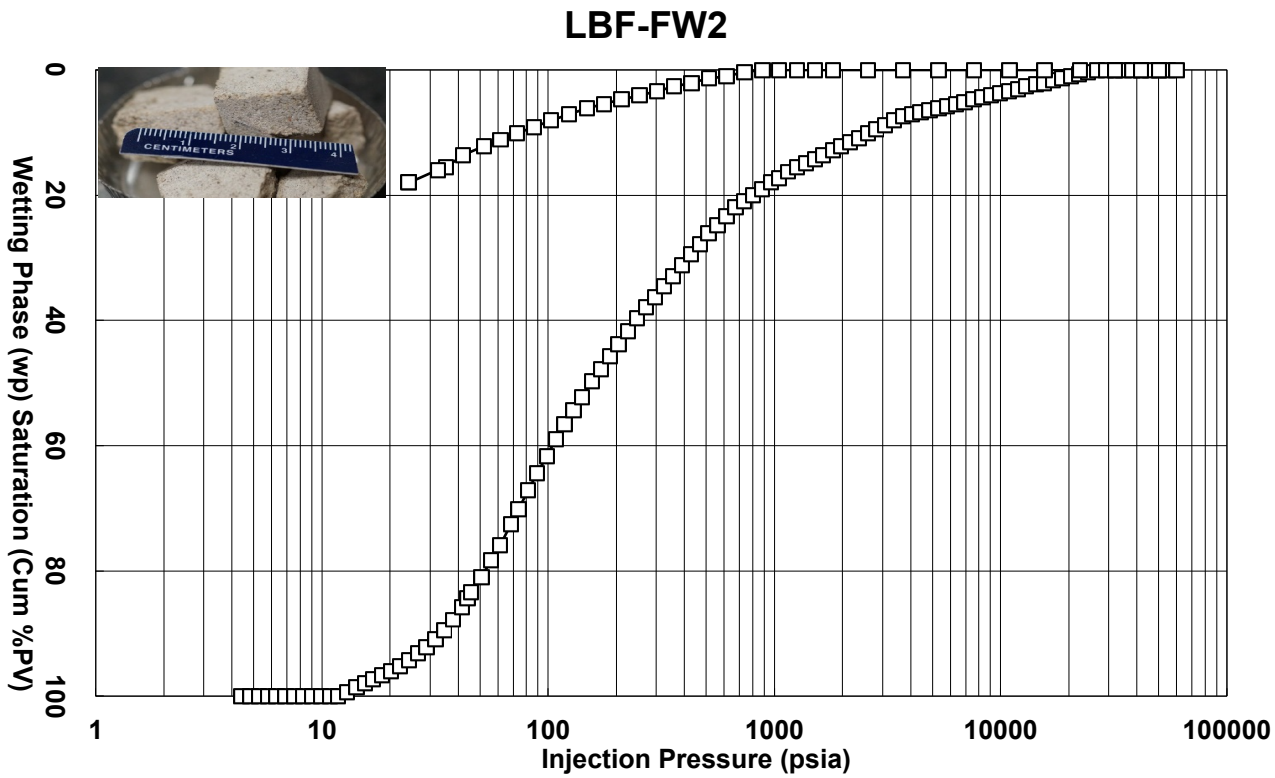
LBF-FW2
0
20
40
60
80
100
Wetting Phase (wp) Saturation (Cum %PV)
1
10
100
1000
10000
100000
Injection Pressure (psia)
CENTIMETERS